



HAL
open science

Absorbing boundary conditions for water wave simulation in the vicinity of a solid body

Jose M. Orellana

► **To cite this version:**

Jose M. Orellana. Absorbing boundary conditions for water wave simulation in the vicinity of a solid body. 2021. hal-02962100v2

HAL Id: hal-02962100

<https://hal.science/hal-02962100v2>

Preprint submitted on 4 Mar 2021 (v2), last revised 29 May 2021 (v5)

HAL is a multi-disciplinary open access archive for the deposit and dissemination of scientific research documents, whether they are published or not. The documents may come from teaching and research institutions in France or abroad, or from public or private research centers.

L'archive ouverte pluridisciplinaire **HAL**, est destinée au dépôt et à la diffusion de documents scientifiques de niveau recherche, publiés ou non, émanant des établissements d'enseignement et de recherche français ou étrangers, des laboratoires publics ou privés.



Absorbing boundary conditions for water wave simulation in the vicinity of a solid body

José Marie Orellana ^a

^a M2N, Department of mathematics, Conservatoire des Arts et Métiers,
292, rue Saint Martin 75141 PARIS Cedex 03 France
E-mail: jose.orellana@lecnam.net (J.M. Orellana)

Abstract. In this paper, we focus on the modelling of the wake of a solid body moving through a body of water. To this end, the flow of an inviscid, barotropic and compressible fluid around the solid body regarded as motionless is examined. The dynamic behaviour of the fluid is analysed by means of a two-dimensional Neumann-Kelvin's coupled model enhanced with capillarity and inertia terms. For computational purposes, the unbounded spatial domain has to be truncated by artificial boundaries. Difficulties arise when it comes to setting appropriate absorbing boundary conditions for a waves propagation problem in a stratified convective fluid media with significant differences between layer properties. Numerical illustrations of the results are given and commented.

Keywords. Absorbing boundary conditions, fluid-structure interaction, water waves propagation, numerical simulations.

2020 Mathematics Subject Classification. 76N99.

This article is a draft (not yet accepted!)

Version française abrégée

Afin de déterminer le sillage d'un corps en mouvement dans une étendue d'eau, on considère l'écoulement d'un fluide non visqueux, barotrope et compressible autour de celui-ci. On étudie la propagation d'une petite perturbation dans ce milieu considéré comme une fluide stratifié en mouvement quasi uniforme à l'aide d'un modèle couplé de type Neumann-Kelvin tenant compte de la viscosité et de l'inertie du fluide. Pour réaliser la simulation numérique, il est nécessaire de délimiter artificiellement le domaine et d'introduire des conditions aux limites absorbantes adaptées. Les résultats obtenus sont analysés et commentés.

1. Introduction

Understanding wave propagation mechanisms on a body of water has long been a subject of interest for many researchers [1–7]. Surface water wave phenomenon is due to the balance between the gravity forces that keep horizontal free surface of the water, the surface tension that keeps the consistency of the air-water interface, the water inertia and the difference between air and water pressure. According to the relevant effect that forces the motion,

the waves are usually divided in gravity waves, capillary waves or pressure waves. Unlike conventional approaches, in our case the waves are regarded as interfacial gravity-capillary waves propagating between two liquid layers with very different properties [1]. The upper layer is the free surface water with an infinitesimal thickness and small characteristic velocity of wave propagation namely, riddle velocity. The lower layer is the inner water with a finite or semi infinite thickness and with a high characteristic velocity of wave propagation namely the speed of sound in water. The waves are usually generated by the movement of the solid body, interacting with its rigid surface and propagating all around it, leading to a wake in its vicinity.

After stating the problem and specifying underlying assumptions, a two dimensional Neumann-Kelvin's coupled modelization enhanced with capillarity and inertia terms is proposed [8]. A linearization around a steady state is performed and different accurate boundary conditions are introduced to carry out the study in an open domain artificially bounded for computational limitation reasons. The variational formulation of the problem is deduced and a finite element approximation in space with a centered finite difference scheme in time are used to approach the solution. Results obtained are illustrated and discussed.

2. Problem statement

Our purpose is to determine the dynamical behaviour of the water surface in the vicinity of a solid body that moves with an horizontal velocity U and with a possible oscillatory displacement. To this end, we examine the flow irrotationnal and unviscid of a compressible and barotropic fluid around the structure seen as fixed. Due to the existence of singularities at contact points between surface solid body and surface of water, and also at underwater angular points [9], the structure is immersed and its shape is simplified to a cylinder. We consider as computational domain a rectangular open domain Ω with a hole of radius R in its center. Its boundary $\partial\Omega = \Gamma_0 \cup \Gamma_1 \cup \Gamma_s \cup \Gamma_2 \cup \Gamma_b$ has unit outward normal vector ν . Γ_0 corresponds to the bottom of the system, Γ_s , to the free surface of the water, Γ_1 and Γ_2 , to the sides through which the water flow enters and leaves Ω and Γ_b , to the rigid body surface (see figure 1). $\partial\Gamma_s$ denotes the edges of Γ_s . A steady flow passes through Ω with horizontal velocity U and a small disturbance is introduced in the fluid as an initial condition.

3. Theoretical modelling

In most cases, to attempt to address wave propagating over a body of water issue, a common formulation of the problem is to find the velocity potential Φ satisfying the Laplace's equation and the vertical displacement of the surface η verifying [1, 2] :

- The kinematic boundary conditions

$$\frac{\partial\Phi}{\partial\nu} = U \cdot \nu \text{ on } \Gamma_0 \cup \Gamma_b \times]0, T[, \quad (1)$$

$$\frac{\partial\Phi}{\partial\nu} = \frac{\partial\eta}{\partial t} + \nabla_s\Phi \cdot \nabla_s\eta \text{ on } \Gamma_s \times]0, T[. \quad (2)$$

- The dynamic boundary conditions

$$\frac{\partial\Phi}{\partial t} - \frac{1}{2} \|\nabla_s\Phi\|^2 - g\eta = 0 \text{ on } \Gamma_s \times]0, T[. \quad (3)$$

- The radiation boundary conditions based on the behavior of the solution in the neighborhood of infinity

$$\nabla\Phi \rightarrow 0 \text{ as } |x| \rightarrow \infty, t \in]0, T[. \quad (4)$$

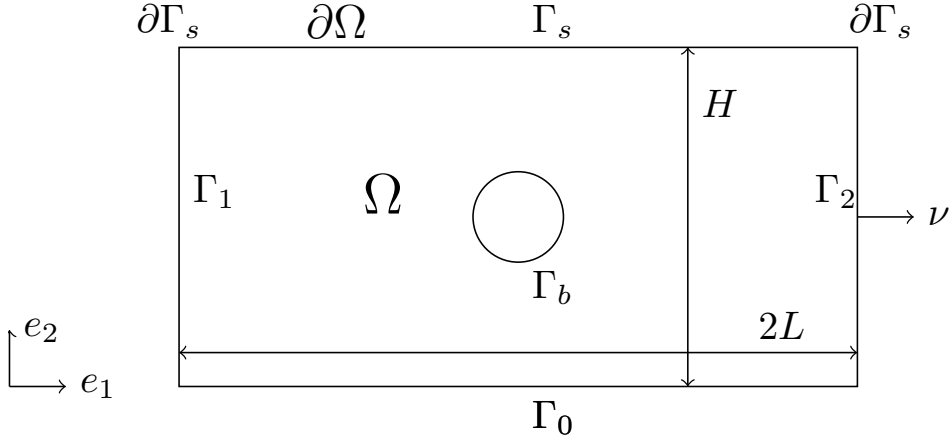


Figure 1. Geometry and notations of the problem.

Incompressibility of the flow is assumed since the water for flow speeds much smaller than the sound speeds in the water and capillarity of the surface is also neglected. In the following, the chosen approach is that of a wave propagation problem with an uniform mean flow in an unbounded stratified fluid waveguide. The propagating medium considered consists of two liquid layers with very different properties and then two models have to be introduced to take these features into account : an inner fluid model and a surface model. The global nonlinear dynamical model obtained is linearized around a main steady state. Therefore the global solution is split into the steady state obtained and a transient one. The lateral boundary conditions are defined separately according to the nature of the state. For the steady flow, the most realistic condition is to fix the normal velocity. For transient flow, non-reflecting boundary conditions have to be prescribed for the inlet and the outlet of Ω in order to avoid any spurious rebounds of the waves reaching the boundaries of the domain.

3.1. Hypotheses and formulation of the global model

3.1.1. Formulation of the inner fluid model

We assume that the flow is characterized by two variables modelling the mass density ρ_{tot} and the velocity potential Φ that satisfy :

- The conservation of mass equation

$$\frac{\partial \rho_{tot}}{\partial t} + \text{div}(\rho_{tot} \nabla \Phi) = 0 \text{ in } \Omega \times]0, T[. \quad (5)$$

- The Bernoulli equation for unsteady compressible potential flow (neglecting gravity effect)

$$\frac{\partial \Phi}{\partial t} + \frac{1}{2} \|\nabla \Phi\|^2 + F(\rho_{tot}) = 0 \text{ in } \Omega \times]0, T[\quad (6)$$

where $F(\rho_{tot}) = \int_{\rho_0}^{\rho_{tot}} \frac{1}{\rho} \cdot \frac{\partial p}{\partial \rho} d\rho + F(\rho_0)$ is the barotropic potential, p , the fluid pressure and T , the simulation time.

3.1.2. Formulation of the surface model

Applying Newton's second law of motion to a infinitesimal small surface element of thickness 2ε that vertically moves η_{tot} , leads to the free surface equilibrium equation :

$$2\varepsilon\rho_{tot}\frac{D^2\eta_{tot}}{Dt^2} = -\rho_{tot}\frac{\partial\Phi}{\partial t} - \frac{\rho_{tot}}{2}\|\nabla_s\Phi\|^2 + \sigma\Delta_s\eta_{tot} - \rho_{tot}g\eta_{tot} \quad \text{in } \Gamma_s \times]0, T[\quad (7)$$

where the forces involved consist in the capillary action $\sigma\Delta_s\eta_{tot}$ with σ the surface tension, the gravity force $-\rho_{tot}g\eta_{tot}$ and the pressure $-\rho_{tot}\partial\Phi/\partial t - \rho_{tot}\|\nabla_s\Phi\|^2/2$. From a mathematical point of view, capillary term stabilizes the partial differential equation [8]. The subscript s indicates that the differential operator is considered locally along a surface namely here Γ_s .

3.1.3. On the interface

The continuity of normal velocity at the interface leads to the relation :

$$\frac{\partial\eta_{tot}}{\partial t} + \nabla_s\Phi \cdot \nabla_s\eta_{tot} = \frac{\partial\Phi}{\partial\nu} \quad \text{in } \Gamma_s \times]0, T[\quad (8)$$

taking account of the rotation of the normal to the surface.

3.2. Linearization of the governing equations

3.2.1. Main background steady state flow

We introduce φ_0 , the velocity potential corresponding to a steady quasi uniform horizontal flow of an incompressible fluid which enters and leaves Ω at constant unit horizontal velocity with normal surface displacement variation along Γ_s regarded as negligible and non penetrability condition on $\Gamma_0 \cup \Gamma_b$ satisfied. This background flow is stationary with respect to the boat which is chosen as frame of reference. φ_0 is the solution to the following problem :

$$\begin{cases} -\Delta\varphi_0 = 0, & \text{in } \Omega \text{ and } \int_{\Gamma_s} \varphi_0 = 0, \\ \frac{\partial\varphi_0}{\partial\nu} = 0, & \text{on } \Gamma_0 \cup \Gamma_b \cup \Gamma_s, \\ \frac{\partial\varphi_0}{\partial\nu} = (e_1 \cdot \nu) & \text{in } \Gamma_1 \cup \Gamma_2. \end{cases} \quad (9)$$

To obtain the related displacement on the surface η_0 of this flow for our model, stationary balance of forces on free surface Eq.(7) along with homogenous Neumann boundary conditions are applied. According to the frame of reference, it leads in stationary case to :

$$\begin{cases} 2\varepsilon\rho_0U^2\nabla_s\varphi_0 \cdot \nabla_s(\nabla_s\varphi_0 \cdot \nabla_s\eta_0) + \sigma\Delta_s\eta_0 - \rho_0g\eta_0 = -\frac{\rho_0}{2}U^2\|\nabla_s\varphi_0\|^2 & \text{in } \Gamma_s, \\ \frac{\partial\eta_0}{\partial\nu_s} = 0 & \text{on } \partial\Gamma_s \end{cases} \quad (10)$$

with ρ_0 , the fluid density and g , the gravity acceleration. The solution of Eq.(9) corresponds to a steady quasi uniform horizontal flow with a digging effect due to the term $-\rho_0U^2\|\nabla_s\varphi_0\|^2/2$ as shown in figure 2. The order of magnitude of free surface strain is about $10^{-3}m$ and therefore negligible in comparison with initial computational domain Ω dimensions.

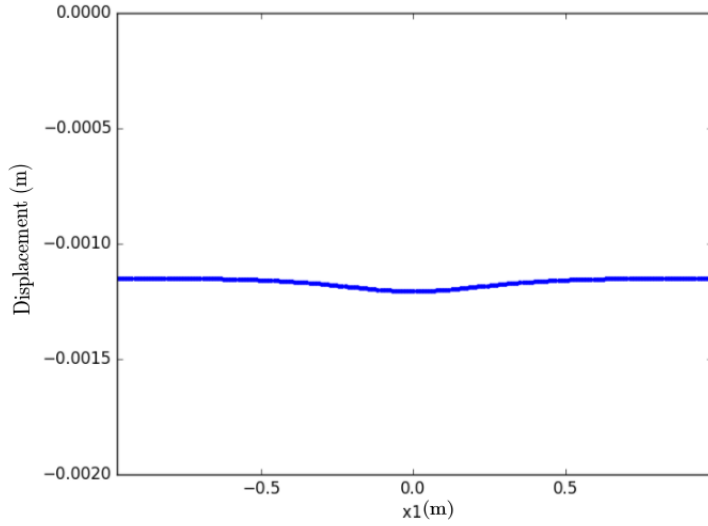


Figure 2. Free surface vertical displacement η_0 (m) solution of Eq.(10) versus x_1 (m) with the ‘digging’ effect.

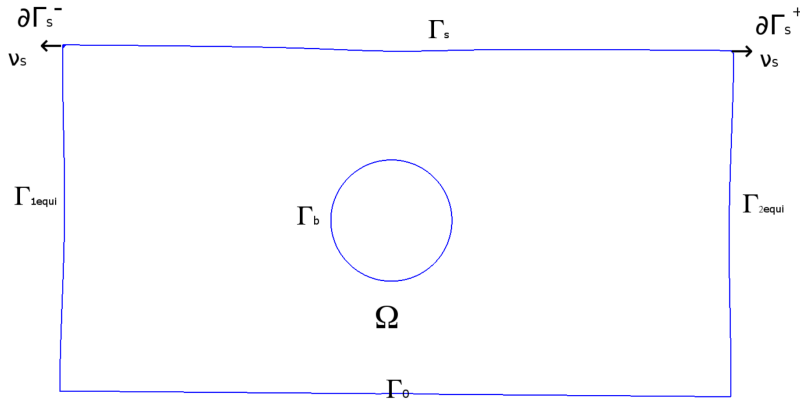


Figure 3. Calculated geometry of the new computational domain in the case of a solid body size large compared to initial computational domain. The digging effect on Γ_s and the inwards bowing of Γ_{1equi} and Γ_{2equi} are more pronounced than in our case.

3.2.2. Transient state

We study the evolution of a small disturbance around the steady state $(\rho_0, \varphi_0, \eta_0)$. The unsteady waves in the fluid are represented by the perturbation functions ρ, φ, η of variables $x(x_1, x_2)$ and t . The problem is formulated with them wherein $\rho_{tot}(x, t) = \rho_0(x) + \rho(x, t)$, $\Phi(x, t) = U\varphi_0(x) + \varphi(x, t)$, $\eta_{tot}(x, t) = \eta_0(x) + \eta(x, t)$. The solution is split into main background steady state component and a transient one. The domain Ω is then cropped by $\Gamma_0, \Gamma_b, \Gamma_s = \eta_0, \Gamma_{1equi}$ and Γ_{2equi} as shown in figure 3 [10]. The new lateral boundaries Γ_{1equi} and Γ_{2equi} correspond to equipotential lines of φ_0 passing respectively through left upper domain corner and right upper corner of Ω . The artificial boundaries are chosen far enough from rigid body to consider that steady state flow is uniform in this area and

so the corners of the new domain are right-angled. The disturbance is so small that it is then reasonable to neglect the non-linear terms in the governing equations Eq.(5)-Eq.(8) to obtain Eq.(11)-Eq.(14). Convective derivatives with flow velocity $U\nabla\varphi_0$ are used to derive linearized equations Eq.(12) and Eq.(13). Hence (ρ, φ, η) are assured to satisfy the linearized enhanced Neumann-Kelvin's model with capillarity :

- The linearized continuity equation

$$\frac{\partial\rho}{\partial t} + U\nabla\rho \cdot \nabla\varphi_0 + \rho_0\Delta\varphi = 0 \quad \text{in } \Omega \times]0, T[. \quad (11)$$

- The linearized momentum equation for the inner fluid

$$\frac{\partial^2\varphi}{\partial t^2} + 2U\nabla\varphi_0 \cdot \nabla \left(\frac{\partial\varphi}{\partial t} \right) + U^2\nabla\varphi_0 \cdot \nabla(\nabla\varphi_0 \cdot \nabla\varphi) - c_f^2\Delta\varphi = 0 \quad \text{in } \Omega \times]0, T[\quad (12)$$

$$\text{given that } \frac{1}{2}|\nabla\varphi_0|^2 + \nabla F(\rho_0) = 0 \quad \text{and} \quad \frac{\partial F(\rho_0)}{\partial\rho_{tot}} = \frac{c_f^2}{\rho_0}.$$

- The linearized momentum equation for the surface fluid

$$2\varepsilon\rho_0 \left(\frac{\partial^2\eta}{\partial t^2} + 2U\nabla_s\varphi_0 \cdot \nabla_s \left(\frac{\partial\eta}{\partial t} \right) + U^2\nabla_s\varphi_0 \cdot \nabla_s (\nabla_s\varphi_0 \cdot \nabla_s\eta) \right) \\ = \sigma\Delta_s\eta - \rho_0g\eta - \rho_0\frac{\partial\varphi}{\partial t} - \rho_0U\nabla_s\varphi_0 \cdot \nabla_s\varphi \quad \text{in } \Gamma_s \times]0, T[\quad (13)$$

where \cdot denotes the scalar product. Since the domain of study was reshaped, $\nabla_s\eta_0$ and $\Delta_s\eta_0$ are set to zero on Γ_s .

- The continuity of normal velocity at the interface

$$\frac{\partial\varphi}{\partial\nu} = \frac{\partial\eta}{\partial t} + U\nabla_s\varphi_0 \cdot \nabla_s\eta \quad \text{in } \Gamma_s \times]0, T[. \quad (14)$$

- The non-penetrability condition leads to homogeneous Neumann boundary condition for φ

$$\frac{\partial\varphi}{\partial\nu} = 0 \quad \text{in } \Gamma_0 \cup \Gamma_b \times]0, T[. \quad (15)$$

- The initial condition corresponding to a disturbance taking place in the fluid: the functions $\varphi(x, 0)$ and $\partial\varphi/\partial t(x, 0)$ are set as Gaussian pulse functions in Ω and the functions $\eta(x, 0)$ and $\partial\eta/\partial t(x, 0)$ are fixed to zero on Γ_s .

3.2.3. Lateral artificial boundary conditions

Finding appropriate artificial boundary conditions able to handle unbounded problems has been an important subject of ongoing research. The main concern is that non-reflecting boundary condition should accurately represents the solution in the infinite domain outside for the arbitrarily bounded domain of study [11]. Absorbing Boundary Conditions [12–14] or Perfectly Match Layer techniques [15–17] result in our case in multiplying the number of equations to solve, not to mention the existence of a background flow that increase the difficulty of the problem. Non-reflecting boundary condition imposed in the following on inner fluid lateral edges is :

$$\frac{\partial\varphi}{\partial t} + \left(U\frac{\partial\varphi_0}{\partial\nu} + c_f \right) \frac{\partial\varphi}{\partial\nu} = 0 \quad \text{in } \Gamma_{1equi} \cup \Gamma_{2equi} \times]0, T[\quad (16)$$

where c_f denotes the speed of sound in the fluid. This relation is consistent with Sommerfeld-like non reflecting boundary condition for a single wave which propagates at the phase velocity c_f corrected by taking account the normal to the boundary velocity component of the

main background steady flow $U\partial\varphi_0/\partial\nu$. As lateral boundaries correspond to equipotential lines of φ_0 , the tangential to the boundary entry velocity of the main steady flow, $\nabla_s\varphi_0$, is equal to zero and then it is assumed that main propagating phenomenon takes place along the normal to the boundary. On the surface bounds $\partial\Gamma_s$ non-reflecting conditions imposed is the natural Sommerfeld-like non reflecting boundary condition,

$$\frac{\partial\eta}{\partial t} + \left(U \frac{\partial\varphi_0}{\partial\nu_s} + c_r \right) \frac{\partial\eta}{\partial\nu_s} = 0 \quad \text{in } \partial\Gamma_s \quad \forall t \in]0, T[\quad (17)$$

where c_r denotes the riddle velocity with $c_r^2 = \sigma/2\rho_0\varepsilon$. It is consistent with the one dimensional non-reflecting boundary condition for a propagating wave at velocity c_r in an uniform background steady flow of velocity $U\partial\varphi_0/\partial\nu_s$. This boundary condition introduces a mathematical specific damping on each boundary nodes of the surface Γ_s in order to attenuate spurious reflecting modes.

4. Solution method

The classical approach for addressing waves propagation in layered media with a wave source close to interfaces by looking for a solution as a superposition of plane waves is not considered in the following [1]. Instead, a weak form of the problem and a finite element formulation are employed.

4.1. Variational formulation and numerical approach

Multiplying Eq.(12) by $\psi \in H^1(\Omega)$ and Eq.(13) by $v \in H^1(\Gamma_s)$ respectively together with Green's formula application lead to the following coupled variational formulation :

$$\begin{aligned} & \text{Find functions } (\varphi, \eta) \in H^1(\Omega) \times H^1(\Gamma_s) \times L^2(]0, T[) \text{ such that } \forall(\psi, v) \in H^1(\Omega) \times H^1(\Gamma_s) \\ & \int_{\Omega} \dot{\varphi}\psi d\tau + U \int_{\Omega} \nabla\varphi_0 \cdot (\nabla\dot{\varphi}\psi - \dot{\varphi}\nabla\psi) d\tau + c_f \int_{\Gamma} \dot{\varphi}\psi d\tau + c_f^2 \int_{\Omega} \nabla\varphi \cdot \nabla\psi d\tau \\ & - U^2 c_f^2 \int_{\Omega} (\nabla\varphi_0 \cdot \nabla\varphi) (\nabla\varphi_0 \cdot \nabla\psi) d\tau - c_f^2 \int_{\Gamma_s} \dot{\eta}\psi d\tau - U c_f^2 \int_{\Gamma_s} \nabla_s\varphi_0 \cdot \nabla_s\eta \psi d\tau = 0 \end{aligned} \quad (18)$$

and

$$\begin{aligned} & 2\varepsilon c_f^2 \int_{\Gamma_s} (\ddot{\eta}v + U\nabla_s\varphi_0 (\nabla_s\dot{\eta}v - \dot{\eta}\nabla_s v) - U^2(\nabla_s\varphi_0 \cdot \nabla_s\eta)(\nabla_s\varphi_0 \cdot \nabla_s v)) d\sigma \\ & - 2\varepsilon c_f^2 U \int_{\Gamma_s} (Uv\Delta_s\varphi_0 (\nabla_s\varphi_0 \cdot \nabla_s\eta) + v\Delta_s\varphi_0\dot{\eta}) d\sigma + \frac{c_f^2}{\rho_0} \int_{\Gamma_s} \sigma\nabla_s\eta \cdot \nabla_s v d\sigma \\ & + \frac{c_f^2}{\rho_0} \int_{\Gamma_s} \rho_0\eta gv d\sigma + c_f^2 \int_{\Gamma_s} \dot{\varphi}v d\sigma - c_f^2 U \int_{\Gamma_s} \nabla_s\varphi_0 \cdot \nabla_s v \varphi + v\Delta_s\varphi_0\varphi d\sigma \\ & + \left[c_f^2 U \frac{\partial\varphi_0}{\partial\nu_s} \varphi v + 2\varepsilon c_f^2 c_r \dot{\eta}v \right]_{\partial\Gamma_s} = 0. \end{aligned} \quad (19)$$

Physical field approximation is performed by classical finite element method. A finite dimension subspace $V_h \subset H^1(\overline{\Omega})$ made of piecewise linear functions on a fixed mesh, characterized by element length h , is considered. Letting $V_h = \text{span}(\varphi_1, \varphi_2, \dots, \varphi_{N1}, \eta_1, \eta_2, \dots, \eta_{N2})$ with φ_i $1 \leq i \leq N1$ and η_i $1 \leq i \leq N2$ finite element shape functions on Ω and on Γ_s respectively.

Calling X the coordinate vector of $\mathcal{X}(\varphi, \eta)$ relative to this basis leads to the recasted algebraic differential linear problem :

Find $X(t) \in R^N$, $N = N1 + N2$, $t \in]0, T[$ such that

$$M\ddot{X} + C\dot{X} + KX = 0 \quad (20)$$

with $X(0), \dot{X}(0)$ prescribed. M, C, K are sparse matrices. Centered finite difference schemes are applied for the time domain approximation in order to avoid numerical instabilities. Finally the problem becomes :

Find $X^{(n)} \in R^N$, $n > 1$, such that

$$A_1 X^{(n+1)} = A_2 X^{(n)} + A_3 X^{(n-1)} \quad (21)$$

where A_1, A_2 et A_3 are sparse matrices depending on M, C, K and Δt with Δt the time step chosen.

The computing process is fully automated. All the geometry operations and meshes are generated and updated automatically according intermediate results by a batch program using Numpy and Scipy Python routines and GMSH [18]. Due to the complexity of weak formulation terms, low-level generic assembly procedures of GETFEM++ is employed to make the assembly of the involved sparse matrices in Eq.(20) [19]. To compute the solution of the large sparse system Eq.(21) a MUMPS solver is used. For the post processing handling, Matplotlib python librairies, PARAVIEW and GMSH are utilized [20]. Mesh convergence study is performed by reducing characteristic size of elements, h , from $h = 10^{-3}$ to $h = 6.25 \times 10^{-5}$. As shown in figures 4 and 5, results converge upon a solution as the mesh density increase. A satisfactory balance between accuracy of results and computing time consuming can be achieved by choosing the value of $h = 1.25 \times 10^{-4}$. For numerical computations, values of parameters of table 4.1 are used.

Parameters	$L(m)$	$H(m)$	$R(m)$	$U(m.s^{-1})$	$\varepsilon(m)$	$\sigma(N.m^{-1})$
Values	1	1	5.10^{-2}	0.15	10^{-3}	0.075

Table 1. Numerical computational values of parameters of the problem

5. Results and comments

Wave propagation phenomenon is monitored by the variation of φ in the inner fluid and the variation of η on the surface respectively. The value of time step chosen is $\Delta t_v = 10^{-5}s$ in order to see properly wave propagation with a velocity of c_f across the extend of the computational domain Ω . As it can be seen on figure 6, reflecting waves appear on the bottom of the domain as on the surface of the immersed solid body where homogeneous Neumann conditions are imposed to modelize non penetrability of the fluid through them. In addition, on both lateral sides of the computational domain no spurious reflecting wave appears to be present. Thanks to hyperbolicity of the problem, in order to verify whether non-reflecting boundary conditions are satisfactory on inner fluid lateral edges Eq.(16), a similar study is carried out according to the same previous calculation criteria on a more expanded computational domain in x_1 direction, sized so as to avoid lateral side spurious reflecting waves on the time range analysed [14]. The new solution obtained is regarded as

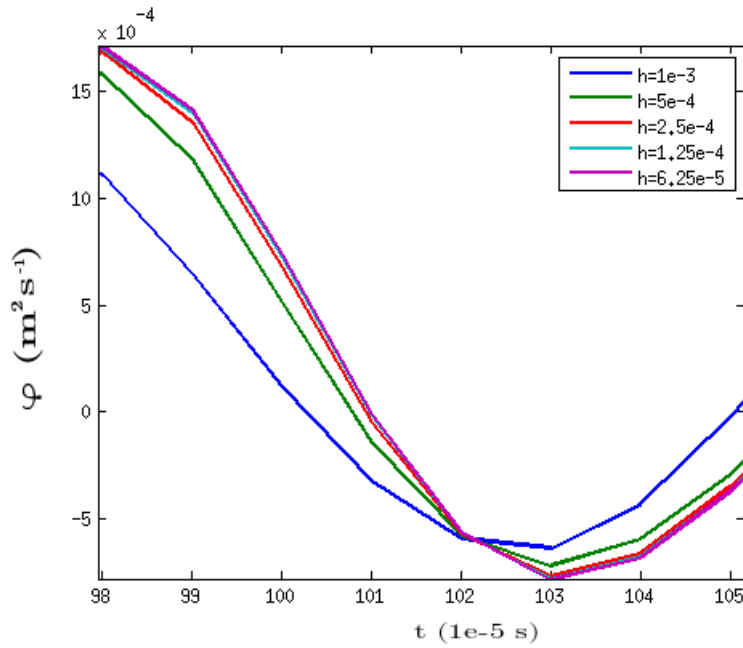


Figure 4. Inner fluid velocity potential φ (m^2s^{-1}) at point of coordinates $(0.5, 0.5)$ versus time ($10^{-5}s$) for different elements sizes of the mesh.

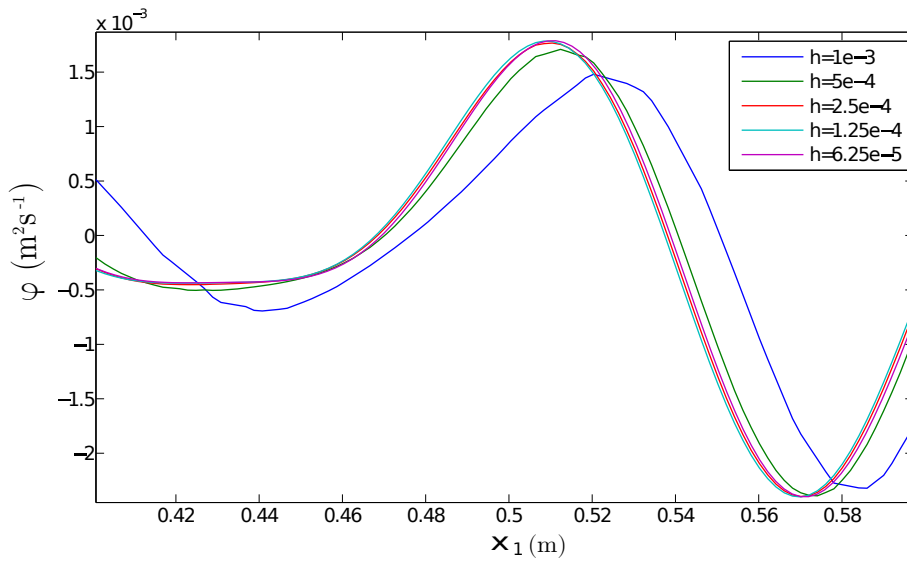


Figure 5. Inner fluid velocity potential φ (m^2s^{-1}) for different mesh densities along a part of the middle line of computational domain (m) at $t = 100\Delta t_v$.

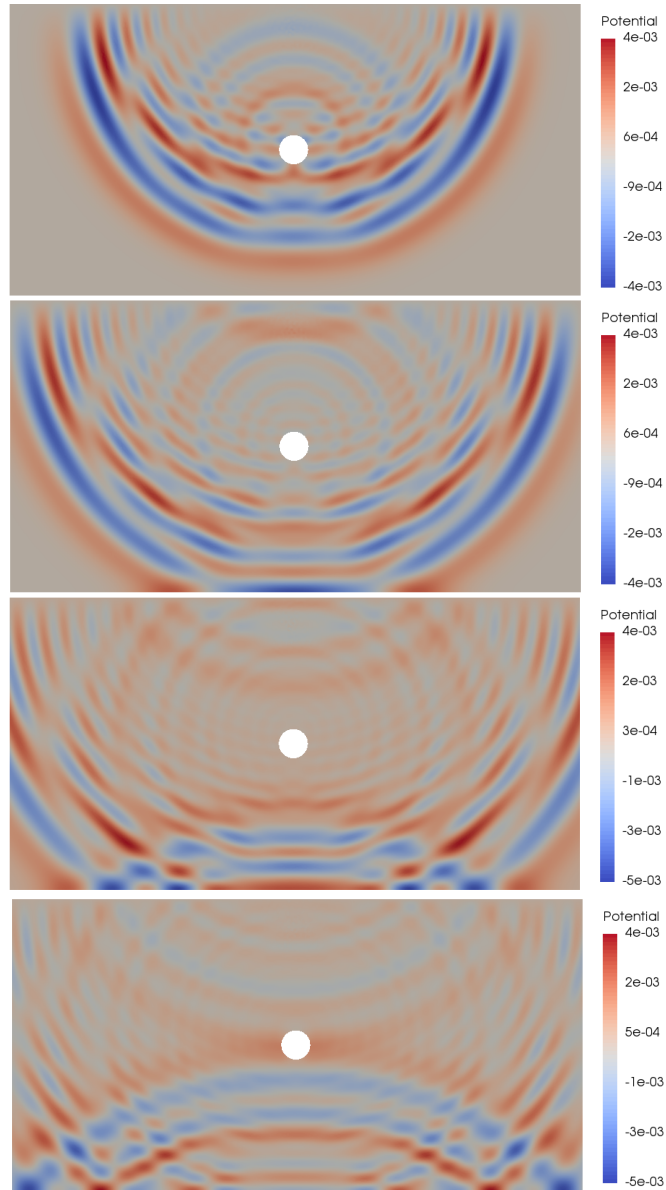


Figure 6. Propagation of velocity potential disturbance φ at times: $t = 80\Delta t_v$, $t = 100\Delta t_v$, $t = 120\Delta t_v$, $t = 140\Delta t_v$. The order of magnitude of initial perturbation is $10^{-2}m^2s^{-1}$.

a reference solution. Both resulting waves are in phase but a variable amplitude difference can be noticed. The wave is slightly reflected especially on its peak of amplitude for times when there are not many interferences. Indeed absorbing boundary conditions chosen are not intended to handle such a situation (see figure 7).

Waves propagation in inner fluid results in deformation of the surface as shown in figures 8 and 9. The corresponding normal displacement η propagates along the surface Γ_s . On

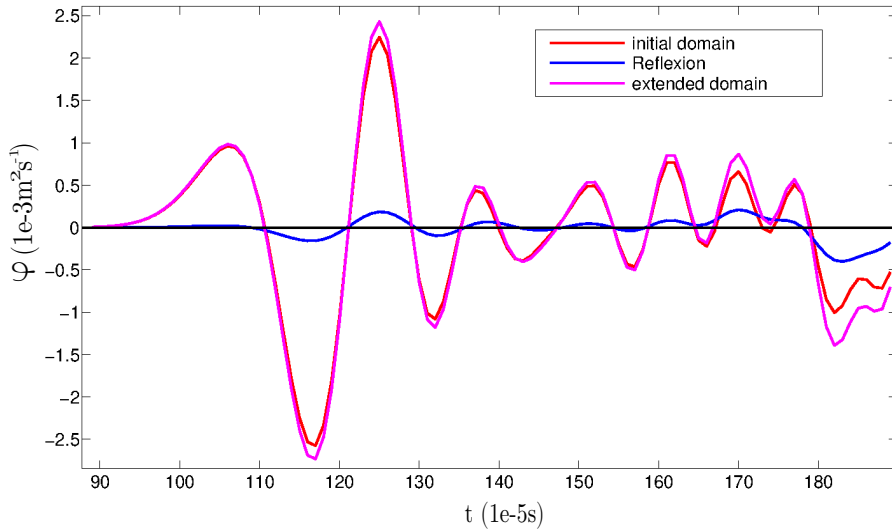


Figure 7. Comparison of inner fluid velocity potentials φ ($10^{-3}m^2s^{-1}$) versus time ($10^{-5}s$) between extended and main computational domain on the middle of right artificial lateral edge.

each side of the surface, $\partial\Gamma_s$, no spurious reflective wave is noticed. In inner fluid layer no wave related with any reflective surface on surface is neither observed (see figure 9). Then lateral boundary conditions introduced Eq.(17) seem to be also adequate to successfully modelize the propagating phenomenon on the surface [10]. Nevertheless the velocity of the phenomenon is the same as in inner fluid layer which is not in complete agreement with surface layer material properties and wave propagation in stratified media theories [1, 6]. The expected value should be closed to the riddle velocity c_r . Normally therefore no surface propagation phenomenon should be observed with time step Δt_v . That's actually what happens when initial disturbance is located just below or on the surface as shown in figure 10. The observed normal displacements η in figures 8 and 9 are not related directly to surface wave propagation, but rather primarily to the potential volume wave propagation in inner fluid layer and to the interface coupling between the potential φ and the normal displacement η on Γ_s given by Eq.(14). The energy transmitted to the surface layer by the inner layer remains stationary over the time range considered. Therefore application of lateral boundary conditions Eq.(17) does not measurably affect the propagation phenomenon and its accuracy can not be estimated with an initial perturbation in inner fluid layer.

Numerical simulations are then carried out in the case of an initial disturbance of the surface with a time step $\Delta t_s = 10^{-2}s$. The functions $\varphi(x, 0)$ and $\partial\varphi/\partial t(x, 0)$ are set to zero in Ω and $\eta(x, 0)$ and $\partial\eta/\partial t(x, 0)$ are introduced as Gaussian pulse functions on Γ_s . Surface waves propagate along Γ_s (see figures 10 and 11) but singularities appear on each side of the surface $\partial\Gamma_s$ as shown on figure 12. In fact due to the significant difference between the wave propagation characteristic velocity values of the surface and inner fluid layers, singularities come out on the intersection between the artificially chosen boundaries of the domain and the two layers' interface when Sommerfeld non reflecting boundary conditions are applied [21]. The non reflecting boundary condition on the lateral edges Eq.(13) has to be changed to handle these difficulties [22]. To this end, as the conditions are to be set for

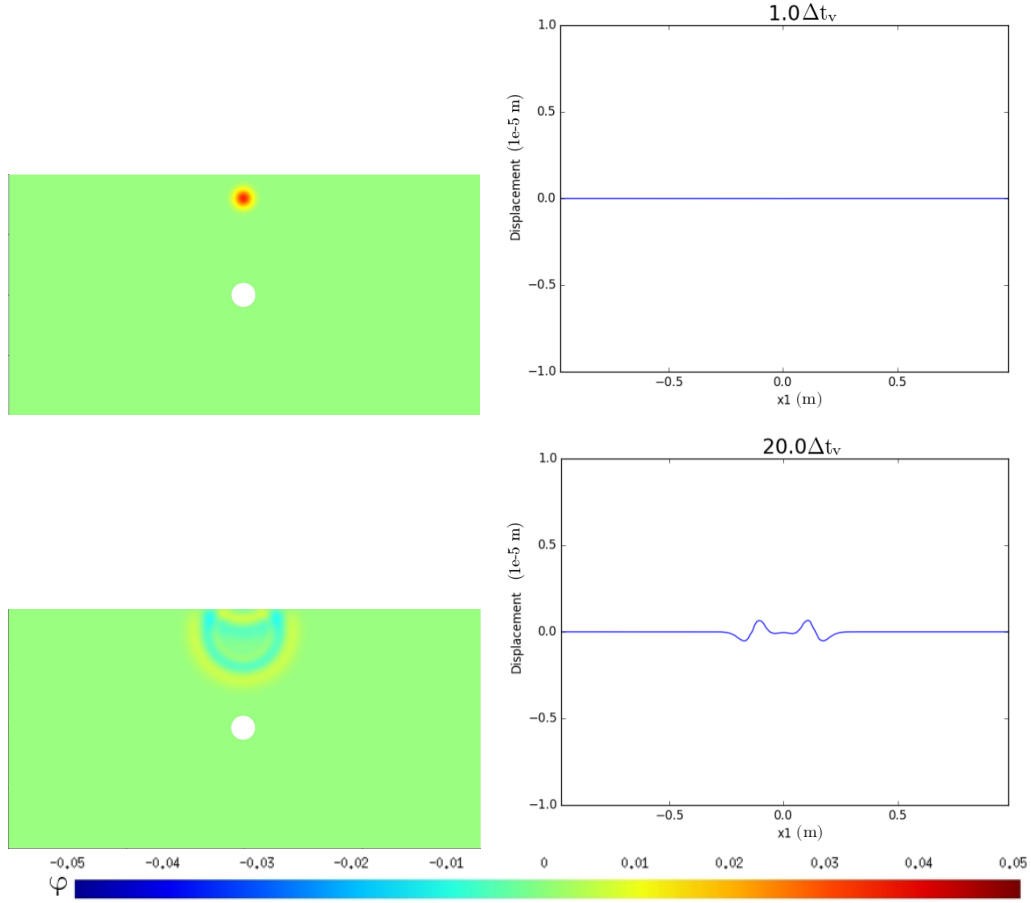


Figure 8. Propagation of disturbance φ in Ω and related normal surface displacement η ($10^{-5}m$) on Γ_s versus x_1 coordinate (m) at times: $t = \Delta t_v$, $t = 20\Delta t_v$. The initial order of magnitude of φ is $10^{-2}m^2s^{-1}$. Its propagating order of magnitude is $10^{-3}m^2s^{-1}$ and the order of magnitude of the normal displacement is $10^{-6}m$.

the points $\partial\Gamma_s$ that belong to the surface Γ_s and to the lateral boundaries Γ_{1equi} or Γ_{2equi} , the equations Eq.(13), Eq.(14) and Eq.(16) are considered to devise the new boundary conditions. The guiding idea is to extend the non reflective boundary condition applied on the lateral boundaries Γ_{1equi} or Γ_{2equi} Eq.(16) to the surface Γ_s intersecting points $\partial\Gamma_s$ Eq.(13) by means of the normal velocity continuity condition Eq.(14). Using the simplifying assumptions $\varphi_0 = x_1$, $s = x_1$ and $(\nu_s \cdot e_1) = \pm 1$ led by choosing Γ_{1equi} and Γ_{2equi} away from rigid body, the following simplified equations must be satisfied on $\partial\Gamma_s$:

$$\frac{\partial^2 \eta}{\partial t^2} + 2U \frac{\partial^2 \eta}{\partial x_1 \partial t} + (U^2 - c_r^2) \frac{\partial^2 \eta}{\partial x_1^2} + \frac{1}{2\varepsilon} \left(\frac{\partial \varphi}{\partial t} + U \frac{\partial \varphi}{\partial x_1} \right) + \frac{g}{2\varepsilon} \eta = 0, \quad (22)$$

$$\frac{\partial \varphi}{\partial x_2} = \frac{\partial \eta}{\partial t} + U \frac{\partial \eta}{\partial x_1}, \quad (23)$$

$$\frac{\partial \varphi}{\partial t} + (U + c_f) \frac{\partial \varphi}{\partial x_1} = 0 \quad \text{on } \Gamma_s \cap \Gamma_{2equi}, \quad (24)$$

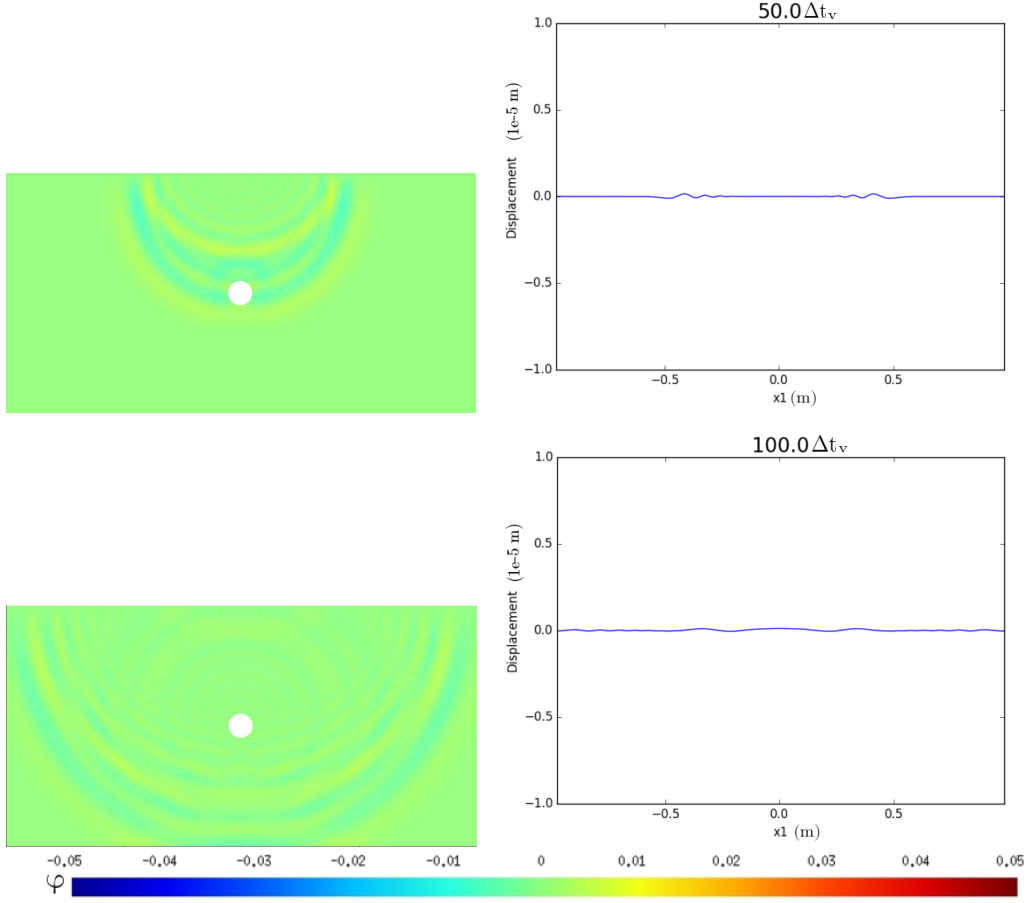


Figure 9. Propagation of disturbance φ in Ω and related normal surface displacement η ($10^{-5}m$) on Γ_s versus $x_1(m)$ coordinate at times: $t = 50\Delta t_v$, $t = 100\Delta t_v$. Its order of magnitude is $10^{-3}m^2s^{-1}$ and corresponding normal displacement η order of magnitude is $10^{-6}m$.

$$\frac{\partial \varphi}{\partial t} + (U - c_f) \frac{\partial \varphi}{\partial x_1} = 0 \quad \text{on } \Gamma_s \cap \Gamma_{1equi}. \quad (25)$$

For the right side (resp. the left side), the solution method consists in derivating first Eq.(24) (resp. Eq.(25)) with respect to x_2 and Eq.(23) with respect to x_1 and t , in order to eliminate partial derivatives of φ . Introducing the resulting expression into Eq.(22) leads, after integrating with respect to time, to the following new boundary condition in cartesian coordinates for each edge,

$$Z^\pm \frac{\partial \eta}{\partial t} + A^\pm \frac{\partial \eta}{\partial x_1} + B^\pm \int_0^t \eta ds + C^\pm \varphi = 0 \quad \text{on } \partial \Gamma_s^\pm \quad (26)$$

with $A^\pm, B^\pm, C^\pm, Z^\pm$ depending on U, c_f, c_r, ϵ, g . The symbol $-$ denotes that condition is on the left boundary of Γ_s and $+$ on the right one. The boundary conditions obtained are said non local in time as they depend not only on the time t but also on entire history of

η on $\partial\Gamma_s$. The second part of variational formulation Eq.(19) becomes within the new non reflective boundary conditions Eq.(26):

$$\begin{aligned}
& 2\epsilon c_f^2 \int_{\Gamma_s} (\ddot{\eta}v + U\nabla_s\varphi_0 (\nabla_s\dot{\eta}v - \dot{\eta}\nabla_s v) - U^2(\nabla_s\varphi_0 \cdot \nabla_s\eta)(\nabla_s\varphi_0 \cdot \nabla_s v)) d\sigma \\
& - 2\epsilon c_f^2 U \int_{\Gamma_s} (Uv\Delta_s\varphi_0 (\nabla_s\varphi_0 \cdot \nabla_s\eta) + v\Delta_s\varphi_0\dot{\eta}) d\sigma + \frac{c_f^2}{\rho_0} \int_{\Gamma_s} \sigma\nabla_s\eta \cdot \nabla_s v d\sigma \\
& + \frac{c_f^2}{\rho_0} \int_{\Gamma_s} \rho_0\eta g v d\sigma + c_f^2 \int_{\Gamma_s} \dot{\varphi} v d\sigma - c_f^2 U \int_{\Gamma_s} \nabla_s\varphi_0 \cdot \nabla_s v \varphi + v\Delta_s\varphi_0\varphi d\sigma \\
& + \left[\left(E^\pm \dot{\eta} + F^\pm \int_0^t \eta ds + G^\pm \varphi \right) v \right]_{\partial\Gamma_s} = 0.
\end{aligned} \tag{27}$$

with E^\pm, F^\pm, G^\pm depending on U, c_f, c_r, ϵ, g . The previous solution method is used to solve the new variational problem Eq.(18) and Eq.(27). For the time domain approximation, centered finite difference scheme is applied for derivatives and trapezoidal rule is used for the integral over time term. The problem becomes finding $X^{(n)} \in R^N$, $n > 1$, such that

$$A_1 X^{(n+1)} = A_2 X^{(n)} + A_3 X^{(n-1)} + F \tag{28}$$

where A_1, A_2 et A_3 are sparse matrices depending on M, C, K and Δt ; F a vector depending on F^\pm and Δt accounting for non local condition term in time Eq.(26) with non zero component corresponding to the surface edges $\partial\Gamma_s$.

A numerical simulation is carried out with an initial surface excitation and a time step Δt_s . Singularities seem to be no longer present on $\partial\Gamma_s$ and waves can get out of computational domain without generating significant spurious reflections (see figure 13). Comparison between the old and the new non reflective boundary condition results is done over two thousand time steps Δt_s to check any singularities (see figure 15). In the same way as the previous case to verify non-reflecting boundary conditions on surface edges Eq.(26), a more expanded computational domain in x_1 direction is chosen to compute a reference solution. Both resulting waves are in phase but a varying amplitude difference can be noticed due to existing spurious reflections (see figure 14) which fade away over time (see figure 13). According to the ratio between the orders of magnitude of the inner fluid potential and the surface displacement noticed in each calculated cases, it comes out that the inner fluid wave propagation effect is not significant in the case of initial disturbance nearby the surface or on the surface itself. Indeed, a velocity potential of order of magnitude of $10^{-3}m^2s^{-1}$ on the surface leads to a normal displacement response of order of magnitude of $10^{-6}m$ in inner fluid initial perturbation case. But in surface initial disturbance case where the order of magnitude of normal displacement is $10^{-6}m$, the velocity potential barely reaches $10^{-6}m^2s^{-1}$ on the surface, the linearity of the model leads to a normal displacement response of $10^{-9}m$, therefore negligible compared to $10^{-6}m$ (see figures 8, 9, 10 and 11). Thus the waves propagate mainly in the surface layer guided in the medium of smaller velocity in totally agreement with wave propagation theories in stratified media. Actually, during surface wave propagation, a small amount of energy is steadily transferred from the surface to inner fluid which is immediately removed from the computational domain as in an incompressible fluid. The velocity potential φ rendering (see figure 11) comes from the superposition of all velocity potential waves generated by the propagating surface wave at all times. Therefore these results can hardly be analysed and used to clearly draw any possible

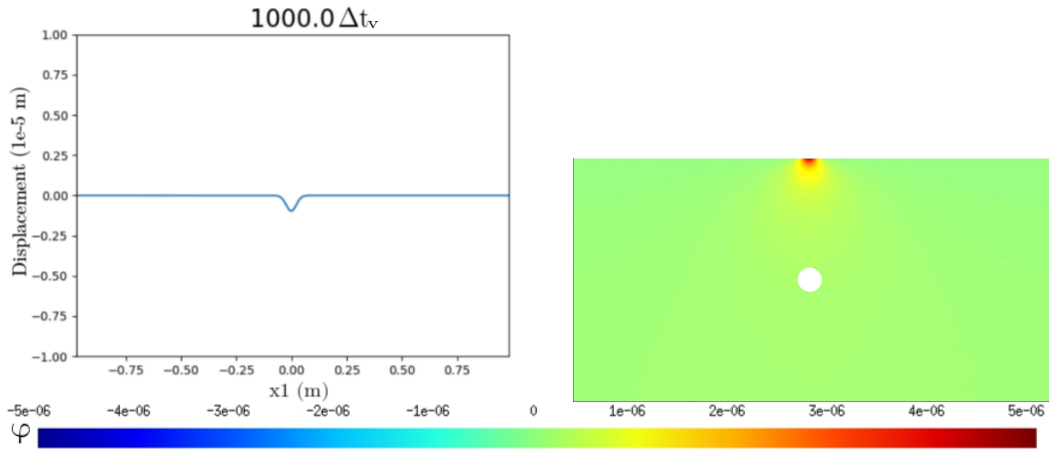


Figure 10. Propagation of normal surface displacement η on Γ_s versus x_1 coordinate and related disturbance φ in Ω at time $t = 1000\Delta t_v = \Delta t_s$. Initial perturbation is located on the surface of the fluid. The order of magnitude of η is $10^{-6}m$. The order of magnitude of the potential φ transmitted to the surface of inner fluid is $10^{-6}m^2s^{-1}$.

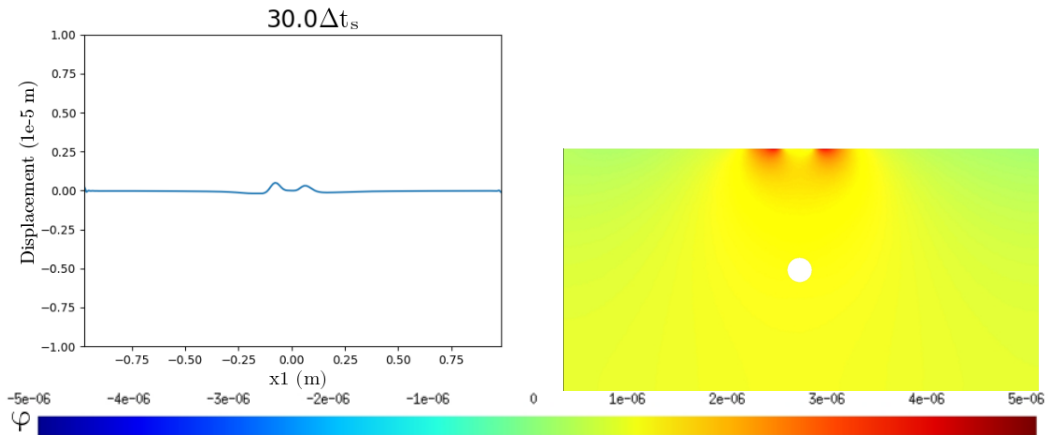


Figure 11. Propagation of normal surface displacement η on Γ_s versus x_1 coordinate and related disturbance φ in Ω at time $t = 30\Delta t_s$. Initial disturbance is located on the surface of the fluid. Order of magnitude of propagating η is $10^{-6}m$. The order of magnitude of the potential φ transmitted to the surface of inner fluid is $10^{-6}m^2s^{-1}$.

conclusions on the compliance of the non reflecting boundary condition chosen Eq.(16) in inner fluid layer.

6. Conclusion

For the modelling of the wake of a solid body moving through a body of water, a wave propagation problem in a convective stratified media is considered. In order to apply standard methods of resolution intended for bounded domains, artificial boundaries are

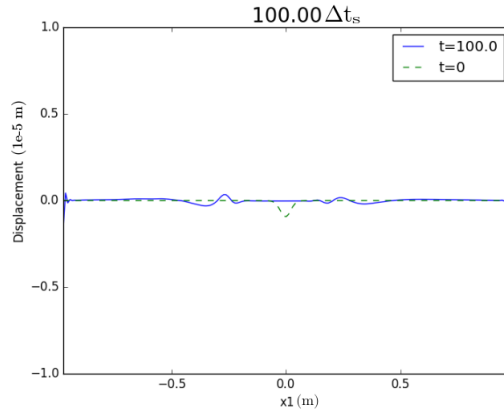


Figure 12. Displacement $\eta(10^{-5}m)$ of the surface Γ_s at time $t = 100\Delta t_s$ versus x_1 coordinate (m). Initial disturbance is located on the surface Γ_s in dash point. Singularities appear on the edges of the surface $\partial\Gamma_s$.

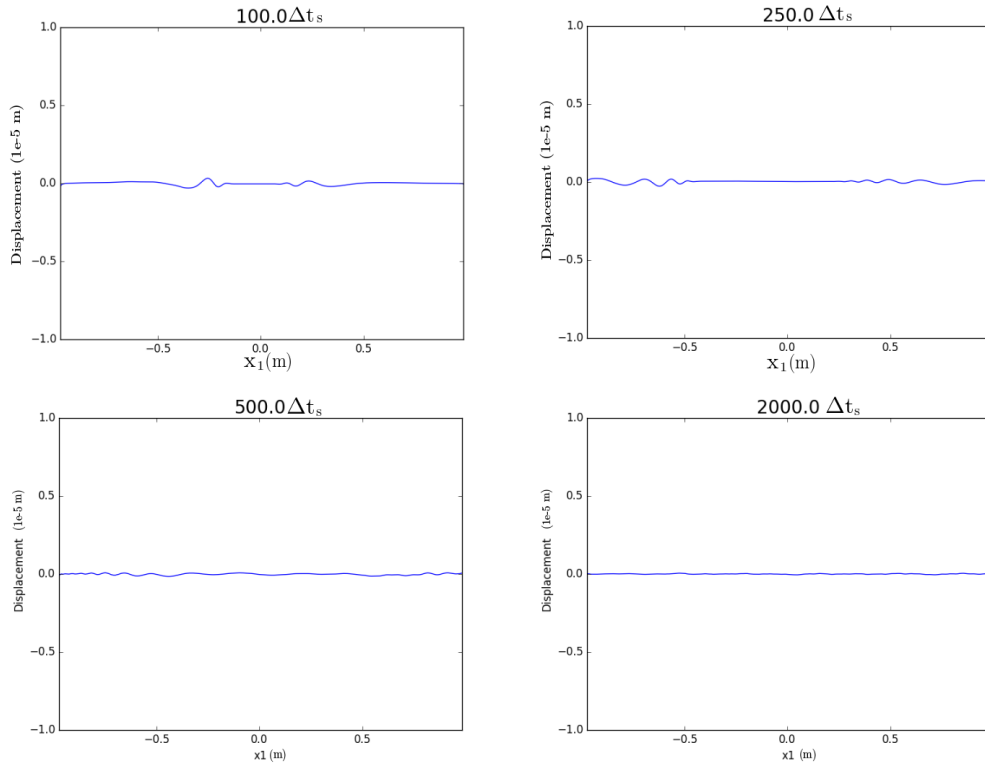


Figure 13. Displacement $\eta(10^{-5}m)$ of the surface Γ_s versus x_1 coordinate (m) at: $t = 100\Delta t_s$, $t = 250\Delta t_s$, $t = 500\Delta t_s$ and $t = 2000\Delta t_s$. Initial disturbance is located on the surface Γ_s . The waves propagate without any singularity on surface edges but spurious reflexions on surface are still present

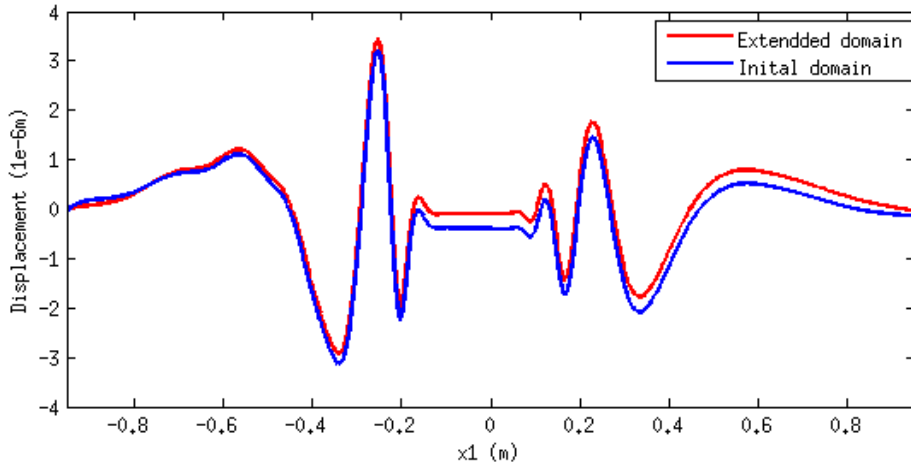


Figure 14. Comparison between normal displacements η ($10^{-6}m$) of surface Γ_s in initial and extended domain cases versus x_1 (m) at $t = 100\Delta t_s$.

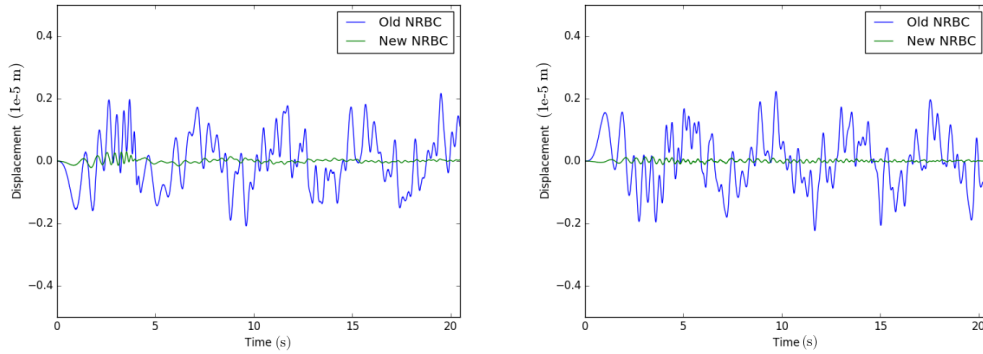


Figure 15. Comparison of the results for displacement η ($10^{-5}m$) at $\partial\Gamma_s^-$ and at $\partial\Gamma_s^+$ obtained by the two non reflective boundary conditions (NRBC) and over simulation time $2000\Delta t_s$.

introduced and appropriate non-reflecting boundary conditions are devised. The significant differences between layer properties make difficult to address the entire problem and a non local in time boundary condition has to be constructed at the interface edges. This work highlighted a complex phenomenon which involves coupled surface and bulk waves propagations at different time scales and with very different orders of magnitude. These features cannot be observed in the assumption of incompressibility of the fluid made in common studies. Further works have to be carried out on non reflecting boundary condition to fully eliminate the reflections of the wave in line with reference results without complicating the formulation of the problem.

Acknowledgment

I would like to thank Professor Philippe Destuynder, at University of La Rochelle (Laboratory LaSIE), for fruitful discussions.

References

- [1] L. Brekhovskikh, *Waves in layered media*, vol. 16, Elsevier, 2012.
- [2] F. Dias, A. Dyachenko, V. Zakharov, “Theory of weakly damped free-surface flows: A new formulation based on potential flow solutions”, *Physics Letters A* **372** (2008), no. 8, p. 1297 - 1302.
- [3] J. Lighthill, *Waves in fluids*, Cambridge university press, 2001.
- [4] M. S. Longuet-Higgins, “Eulerian and Lagrangian aspects of surface waves”, *Journal of Fluid Mechanics* **173** (1986), p. 683–707.
- [5] J. W. Miles, “On the generation of surface waves by shear flows”, *Journal of Fluid Mechanics* **3** (1957), no. 02, p. 185-204.
- [6] A. H. Nayfeh, *Wave propagation in layered anisotropic media: With application to composites*, Elsevier, 1995.
- [7] J. Stocker, “Water waves”, *Pure and Applied Mathematics* **9** (1957), p. 291-314.
- [8] P. Destuynder, C. Fabre, “A discussion on Neumann–Kelvin’s model for progressive water waves”, *Applicable Analysis* **90** (2011), no. 12, p. 1851-1876.
- [9] P. Destuynder, C. Fabre, “Modélisation du comportement hydrodynamique des bateaux”, Lecture, Jun 2012.
- [10] D. Bissengue, O. Wilk, “Conditions aux limites transparentes et modélisation des vagues de surface dans un écoulement”, 2012.
- [11] D. Givoli, *Numerical methods for problems in infinite domains*, vol. 33, Elsevier, 2013.
- [12] B. Engquist, A. Majda, “Absorbing boundary conditions for numerical simulation of waves”, *Proceedings of the National Academy of Sciences* **74** (1977), no. 5, p. 1765-1766.
- [13] L. Halpern, “Absorbing boundary conditions for the discretization schemes of the one-dimensional wave equation”, *Mathematics of Computation* **38** (1982), no. 158, p. 415-429.
- [14] E. Bécache, D. Givoli, T. Hagstrom, “High-order absorbing boundary conditions for anisotropic and convective wave equations”, *Journal of Computational Physics* **229** (2010), no. 4, p. 1099-1129.
- [15] E. Bécache, A. B.-B. Dhia, G. Legendre, “Perfectly matched layers for the convected Helmholtz equation”, *SIAM Journal on Numerical Analysis* **42** (2004), no. 1, p. 409-433.
- [16] J.-P. Berenger, “A perfectly matched layer for the absorption of electromagnetic waves”, *Journal of computational physics* **114** (1994), no. 2, p. 185-200.
- [17] A. Bermúdez, L. Hervella-Nieto, A. Prieto, R. Rodrí *et al.*, “An optimal perfectly matched layer with unbounded absorbing function for time-harmonic acoustic scattering problems”, *Journal of Computational Physics* **223** (2007), no. 2, p. 469-488.
- [18] C. Geuzaine, J.-F. Remacle, “Gmsh: A 3-D finite element mesh generator with built-in pre-and post-processing facilities”, *International journal for numerical methods in engineering* **79** (2009), no. 11, p. 1309-1331.
- [19] Y. Renard, K. Poullos, “GetFEM: Automated FE modeling of multiphysics problems based on a generic weak form language”, *ACM Transactions on Mathematical Software (TOMS)* **47** (2020), no. 1, p. 1-31.
- [20] J. Ahrens, B. Geveci, C. Law, “Paraview: An end-user tool for large data visualization”, *The visualization handbook* **717** (2005), no. 8.
- [21] P. Destuynder, C. Fabre, “Singularities occurring in multimaterials with transparent boundary conditions”, *Quarterly of Applied Mathematics* **74** (2016), no. 3, p. 443-463.
- [22] M. López de Silanes *et al.*, *Fourteenth International Conference Zaragoza–Pau on Mathematics and its Applications: Jaca (Spain), September 12*, vol. 41, Prensas de la Universidad de Zaragoza, 2018, 149-158 pages.